ACS APPLIED MATERIALS & INTERFACES

Research Article

www.acsami.org

Synthesis of Strongly Fluorescent Molybdenum Disulfide Nanosheets for Cell-Targeted Labeling

Nan Wang,[†] Fang Wei,[‡] Yuhang Qi,[†] Hongxiang Li,[†] Xin Lu,[§] Guoqiang Zhao,[§] and Qun Xu*,[†]

[†]College of Materials Science and Engineering, Zhengzhou University, Zhengzhou 450052, China

[‡]College of Life Sciences, Zhengzhou University, Zhengzhou 450052, China

[§]Basic Medical College, Zhengzhou University, Zhengzhou 450052, China

Supporting Information

ABSTRACT: MoS_2 nanosheets with polydispersity of the lateral dimensions from natural mineral molybdenite have been prepared in the emulsions microenvironment built by the water/surfactant/CO_2 system. The size, thickness, and atomic structure are characterized by transmission electron microscopy (TEM), atomic force microscopy (AFM), and laser-scattering particle size analysis. Meanwhile, by the analysis of photoluminescence spectroscopy and microscope, the MoS_2 nanosheets with smaller lateral dimensions exhibit extraordinary photoluminescence properties different from those with relatively larger lateral dimensions. The discovery of the excitation dependent photoluminescence for MoS_2 nanosheets makes them potentially of interests for the applications in optoelectronics and biology. Moreover, we demonstrate that the fabricated MoS_2 nanosheets can be a nontoxic fluorescent label for cell-targeted labeling application.

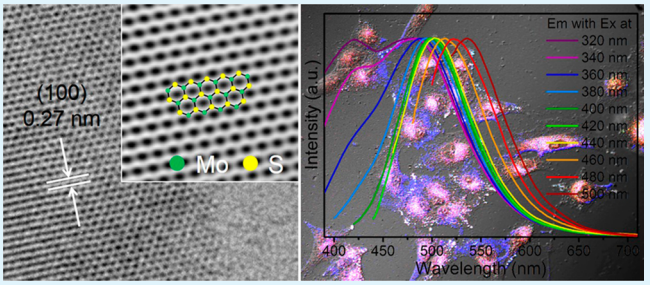

KEYWORDS: *photoluminescence, cell labeling, molybdenum disulfide, nanosheets, lateral dimensions control*

1. INTRODUCTION

Layered two-dimensional (2D) nanomaterials[1−7] have been extensively studied in the field of nanoscience. Due to the similar structure with graphene,[2,5] significant developments have likewise been spearheaded by research into molybdenum disulfide (MoS_2),[8] which has manifested unique physical and chemical properties[6,9−12] compared to their bulk forms, spurring intense scientific interests. In principle, each 2D crystal layer of MoS_2 consists of two planes of hexagonally arranged sulfur atoms separated by an intermediate plane of hexagonally arranged molybdenum atoms, with the covalently bonded S−Mo−S atoms in a trigonal prismatic arrangement forming a hexagonal crystal structure.[13−15] As with graphite, these adjacent MoS_2 layers stack into 3D crystals via weak van der Waals interactions, which makes it possible to fabricate the single- or few-layer MoS_2 nanosheets through different top-down exfoliation methods including micromechanical exfoliation,[3,16] liquid-phase exfoliation,[17−21] ion intercalation technique.[22−24]

These as-fabricated MoS_2 nanosheets show great promise for potential applications in photoelectronic devices,[9,25−27] sensors,[28,29] energy storage devices,[30] and catalysis.[31,32] Several recent studies have shown that MoS_2 enable an indirect-to-direct bandgap transition due to the hybridization between p_z orbitals of S atoms and d orbitals of Mo atoms, when its thickness is thinned to monolayer. This transition results in the giant enhancement of its photoluminescence (PL) efficiency in MoS_2 monolayers, which makes it very interesting for many optoelectronic applications.[33−36] Meanwhile, the direct nature of the band gap opens a realm of electronic and photonic possibilities that allows fabrication of MoS_2 transistors, photodetectors, and even LEDs.[9] In addition, recent study also proves that it could be as a promising candidate for the catalyst of the hydrogen evolution reaction (HER).[37−39] Predictably, the success of MoS_2 in these fields opens up new prospects for technological breakthroughs and encourages the exploration of MoS_2 for new research fields, for example, biology including biomedicine, biosensors, and cell-targeted labeling.[40] However, up to now, there have been only a limited number of reports[41−45] using MoS_2 in the field of biology.

In this work, we explored the potential of the functionalized MoS_2 nanosheets as a promising cell-targeted labeling in the biological applications. MoS_2 nanosheets are synthesized in the emulsions microenvironment built by the water/surfactant/CO_2 system.[46,47] CO_2 can assist surfactant−water solutions in building the emulsions microenvironment as the continuous phase, and the phase behavior of emulsions microenvironment can be manipulated by tuning the physical properties of supercritical CO_2,[46−48] which might be critical to achieve the exfoliation of MoS_2. The surfactant used in the system is

Received: August 8, 2014
Accepted: November 7, 2014
Published: November 7, 2014

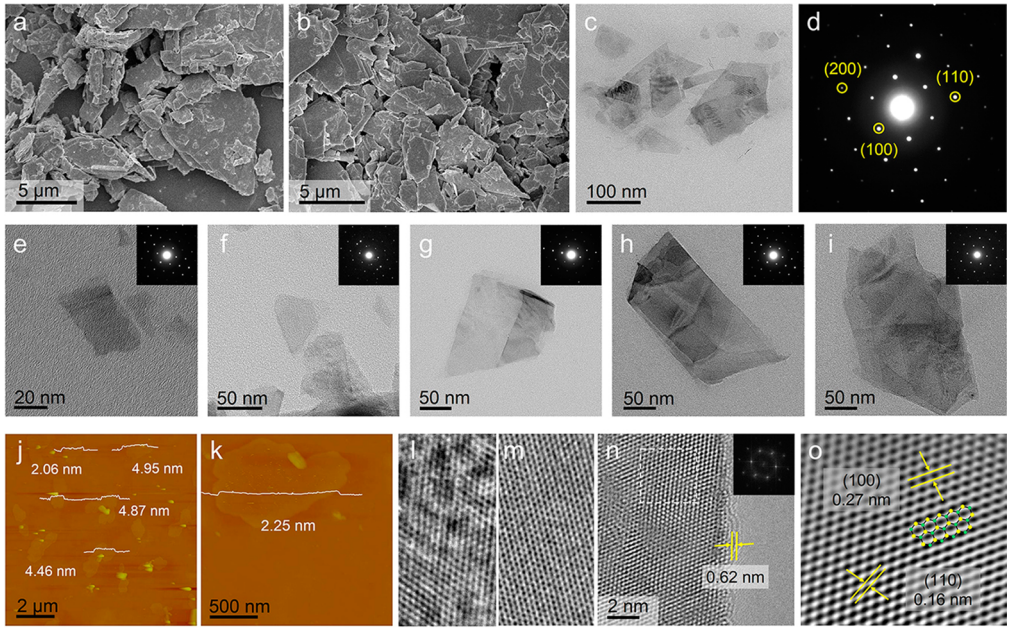

Figure 1. (a, b) SEM images of the starting MoS_2 powder and the sediment collected after centrifugation. (c, d) Low-magnification TEM image and SAED pattern of MoS_2 nanosheets. (e–i) High-magnification TEM images of MoS_2 nanosheets. The insets are the SAED patterns of the corresponding MoS_2 nanosheets. (j, k) AFM images of exfoliated MoS_2 nanosheets on Si/SiO_2 substrate. (l–n) HRTEM images of a few-layer MoS_2 nanosheet. (o) A filtered image of part of the region enclosed by the white square of (n).

polyvinylpyrrolidone (PVP), which is a nonionic, nontoxic, water-soluble, and biocompatible polymer surfactant. As a branched polymer, PVP, with the excellent wetting property and 2D plane structure, can adsorb on the surface of MoS_2 nanosheets and increases their physiological stability and biocompatibility.[20] Moreover, the selected MoS_2 nanosheets with smaller lateral dimensions exhibit extraordinary photoluminescence properties different from those with relatively larger lateral dimensions. The discovery of the excitation dependent photoluminescence of the MoS_2 nanosheets makes them potentially of interests for the applications in optoelectronics and biology. By analysis of the toxicity of functionalized MoS_2 nanosheets with smaller lateral dimensions to cells, we demonstrated that the functionalized MoS_2 nanosheets show the negligible toxicity to cell, indicating the great potential of implementing MoS_2 as a novel type of fluorescence labeling in biological systems. More importantly, the PL modulation of functionalized MoS_2 nanosheets in cancer cells provides the prospects of using 2D MoS_2 nanosheets for optically monitoring biological systems.

2. EXPERIMENTAL SECTION

2.1. Materials. Commercially available MoS_2 Powder was purchased from Sigma-Aldrich (Fluka, Product Number 69860). According to the description of products, the starting MoS_2 powder has representative lateral particle sizes in the range of 6–40 μm. Polyvinylpyrrolidone (PVP) was purchased from STREM CHEMICALS (Fluka, Product Number: 07-1815). Ethanol used in all experiments was purchased from Sinopharm Chemical Reagent Co., Ltd. (China) and used without further purification since the reagent is of analytical grade. Aqueous solution was prepared with double-distilled water.

2.2. Preparation of MoS_2 Nanosheets with Controllable Lateral Dimensions. All chemical reagents were of analytical grade and were used without further purification. MoS_2 powder was added at a concentration of 25 mg/mL to 10 mL of the water/ethanol (1:1) mixtures, in which 200 mg PVP was added beforehand, and then the mixture was sonicated in an ice bath for 2 h. The dispersion was quickly added into the supercritical CO_2 apparatus composed mainly of a stainless steel autoclave (50 mL) with a heating jacket and a temperature controller. The autoclave was heated to 313.2 K, and CO_2 was then charged into the autoclave to the desired pressure (16 MPa) under stirring. After a reaction time of 3 h, the gas was released. Finally, the as-produced dispersion was sonicated for an additional 3 h, and then the dispersion was centrifuged at 3000 rpm for 15 min to remove aggregates. The supernatant (top three-quarters of the centrifuged dispersion) was collected by pipet. For the MoS_2 nanosheets with smaller lateral dimensions, the resulting products were collected by centrifugation at 11000 rpm for 30 min.

2.3. Characterization of As-Prepared Materials. The morphologies of MoS_2 powder and sediment were characterized by field-emission SEM (JEOR JSM-6700F). Tapping-mode AFM (Nanoscope IIIA), HRTEM (JEOL JEM-2100F), and TEM (JEOL JEM-2100) were used to study the morphology of the nanomaterials. UV–vis spectra (Shimadzu UV-240/PC) were measured to evaluate MoS_2 dispersions concentration. The PL properties of MoS_2 nanosheets were investigated by PL spectra (Horiba Fluorolog-3) and fluorescence microscope (Olympus IX81).

2.4. Assay of Cell Proliferation Capacity after MoS_2 Treatment. The 3-(4, 5)-dimethylth-iahiazo(-z-y1)-3,5-diphenytetrazoliumromide (MTT) assay is considered to evaluate cell proliferation for testing cytotoxicity.[54] We performed a standard MTT method to assess the proliferation capacity of the U251 glioblastoma cells treated with MoS_2. MoS_2 nanosheets used in the assay are these nanosheets with smaller lateral dimensions (below 120 nm) collected by centrifugation at 11000 rpm. After reaching the exponential growth phase, the U251 glioblastoma cells were harvested to prepare cell suspension. Then, the cells were seeded at a density of 1×10^4 cells/well in a 96-well microwell plates, after incubation 12 h, the MoS_2 were added to the microwell plates, and the final concentrations of the MoS_2 were from 25 μg/mL to 500 μg/mL. The culture medium was removed after incubating for 48 h, and 200 μL of the MTT solution (final concentration: 0.5 mg/mL; Sigma-Aldrich Co.) was added. The cells were then incubated for 4 h, and 150 μL of dimethyl sulfoxide (DMSO) was added, the plates were incubated for another 15 min. Finally the absorbance was measured at 570 nm on a microplate spctrophotometer (Bio Tek Instrument Inc., USA). All experiments

were performed three times, and the U251 glioblastoma cells without MoS_2 treatment were served as controls.

2.5. Assay of Cell Viability after MoS_2 Treatment. MoS_2 nanosheets used in the assay are these nanosheets with smaller lateral dimensions (below 120 nm) collected by centrifugation at 11000 rpm. The cell viability of the U251 glioblastoma cells treated with MoS_2 was assessed using a fluorescein diacetate (FDA) (Sigma-Aldrich Co., St. Louis, MO, USA) and propidium iodide (PI) (Sigma-Aldrich Co.) double-staining protocol.[55] The U251 cells were seeded at a density of 2×10^4 cells/well in a 24-well plate, after incubation 12 h, MoS_2 were added to the 24-well plate, and the final concentrations of the MoS_2 varied from 25 μg/mL to 500 μg/mL. Subsequently, FDA solution with a final concentration of 1 μg/mL and PI solution with a final concentration of 20 μg/mL were successively introduced into the culture plates after being cultured for 48 h. The cellular viability was then analyzed by counting the live and the dead cells after incubation for 10 min at room temperature. The samples were analyzed with an inverted fluorescence microscope (Eclipse TE 2000-U, Nikon, Kyoto, Japan) equipped with a high-resolution CCD camera (CV-S3200, JAI Co., Japan). The living cells were stained green by FDA, whereas the dead cells were stained red by fluorescent dye PI. The U251 cells without MoS_2 treatment served as controls.

2.6. Fluorescent Staining of Apoptotic Cells. To visualize apoptotic cells, the cells treated with MoS_2 with smaller lateral dimensions below 120 nm were fixed with 4% paraformaldehyde for 15 min, and then stained with bisbenzimide dye Hoechst H33258 solution (concentration: 2 μg/mL) for 10 min at room temperature. The stained cells were rinsed with PBS for three times, and then observed via an inverted fluorescence microscope equipped with a high-resolution CCD camera. The cells without MoS_2 treatment were used as controls.

2.7. Cell-Targeted Labeling. Two pieces of round cover glass (13 mm diameter, VWR International) were placed in a 12-well plate with 1 cover glass and 1 mL of DMEM culture medium per well. A total of 2×10^4 cells were plated in each well of that 12-well plate. The cells were incubated at 37 °C overnight to adhere on the cover glass. MoS_2 with smaller lateral dimensions below 120 nm were added in culture medium, and then the cells were incubated at 37 °C for 24 h. After incubation, the cells on two cover glasses were washed with 1 mL of 1 × PBS separately. Cells were fixed using 4% paraformaldehyde at room temperature for 5 min. Then cells on cover glasses were washed with 1 mL of 1 × PBS and mounted with Vectashield antifade mounting media. Cellular images were taken using the Olympus IX81 inverted research microscope equipped with the Olympus DP70 Color/Black and White camera (Olympus, America). An Olympus U-RFL-T power supply unit with a mercury lamp was used as the fluorescence light source.

3. RESULTS AND DISCUSSION

The 2D MoS_2 nanosheets were fabricated from MoS_2 bulk crystals in the emulsions microenvironment built by the CO_2/PVP/water system. Compared with the initial MoS_2 powder (Figure 1a), the sediment (Figure 1b) separated after centrifugation contains sheets with the smaller lateral dimensions and thicknesses, which make it possible to infer that the smaller and thinner MoS_2 nanosheets can be tore from the crystallites via this fabrication procedure. Transmission electron microscopy (TEM) analysis was performed to demonstrate that a large quantity of ultrathin nanosheets with lateral dimensions varying from tens to hundreds of nanometers exist in MoS_2 supernatant collected via centrifugation at 3000 rpm, showing the polydispersity of their lateral dimensions (Figure 1c–i). These MoS_2 nanosheets turn slightly transparent to the electron beam because of its ultrathin structure. The corresponding selected area electron diffraction (SAED) patterns of the 2D MoS_2 nanosheets indicate their typical 6-fold symmetry of highly crystalline structure and that individual sheets consist of a single crystal domain. In addition, atomic force microscopic (AFM) characterization also confirmed that these as-prepared MoS_2 nanosheets were polydisperse in lateral dimensions. By the analysis based on AFM measurement, these MoS_2 nanosheets have different thicknesses with the majority in the range of 2–5 nm, confirming that bulk MoS_2 crystals were exfoliated into ultrathin nanosheets.

Further examination of the nature of the nanosheets was performed by high-resolution transmission electron microscopy (HRTEM), providing more detailed structural information. Significant nonuniformities on the plane of MoS_2 can be seen in Figure 1l, probably becaus of the stack of free PVP in dispersions on the plane of the 2D MoS_2 in the process of preparing HRTEM samples. However, as shown in Figure 1m, these redundant PVP can be removed by the repeating the washing and centrifugation steps.[20] Figure 1n shows the hexagonally symmetric lattice structure of a bilayer MoS_2, presenting two dark fringes with a space of 0.62 nm, in good agreement with the interlayer distance of MoS_2. The inset depicts a Fast Fourier transform (FFT) of this image, which is equivalent to an electron diffraction pattern. The filtered image of part of the region indicated by the white square in Figure 1n is shown in Figure 1o. This filtered image is of atomic resolution and clearly illustrates the hexagonal nature of MoS_2 with the lattice spacing of 0.27 nm ((100) plane) and 0.16 nm ((110) plane), which is consistent with the typical atomic structure of MoS_2 composed of hexagons with Mo and S_2 atoms alternately located at six corners.

The analyses of morphology and dimension of MoS_2 nanosheets demonstrate the polydispersity of their lateral dimensions. It makes possible to achieve the controllable selection in the lateral dimension by adjusting the centrifugation rate.[17] As shown in Figure 2a, the MoS_2 nanosheets with the smaller lateral dimensions below 120 nm were successfully selected at the centrifugation rate of 11000 rpm. Apart from the nanosheets with the dimension at tens nanometres, a small quantity of extremely small MoS_2 nanosheets below 10 nm are observed in Figure 2b, c. Meanwhile, the analysis of lateral

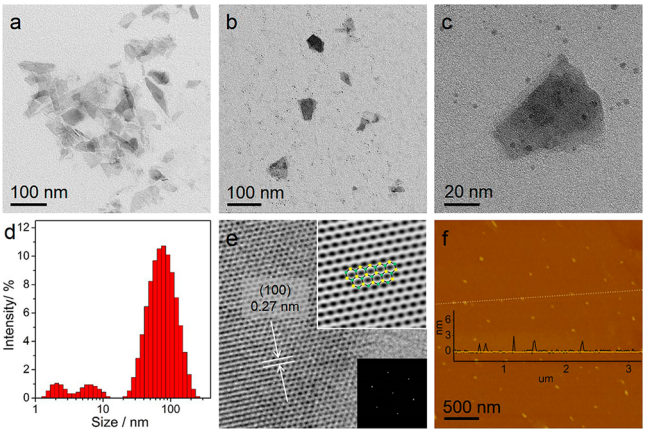

Figure 2. (a–c) TEM images of MoS_2 nanosheets with smaller lateral dimensions collected by centrifugation at 11000 rpm. (d) The lateral dimension distribution of these MoS_2 nanosheets. (e) A HRTEM image of a sample area on a corner of a MoS_2 nanosheet with smaller lateral dimensions. The inset is a filtered image of part of the image e and Fast Fourier transform of the image e, respectively. (f) AFM images of MoS_2 nanosheets with smaller lateral dimensions.

dimension distribution in Figure 2d also shows the polydisperse feature of their lateral dimensions, which range mainly between 30 and 120 nm, and are below 10 nm only in very small amounts. HRTEM is utilized to reveal the crystal structure of the MoS_2 nanosheets with smaller lateral dimensions. Figure 2e shows the HRTEM image of a MoS_2 nanosheet shown in Figure 2c, in which the structural uniformity on the plane of MoS_2 is observed and a lattice fringe spacing of 0.27 nm ((100) plane) is clearly identified. The inset in Figure 2e shows a near perfect planar 2H-MoS_2 and depicts the Fast Fourier transform of this region, which confirms the hexagonal honeycomb structures. AFM is used for assessing the lateral dimensions and thicknesses of these MoS_2. Figure 2f shows the typical AFM image of MoS_2 nanosheets with smaller lateral dimensions. The products consist of small individual particles. AFM line analysis of some MoS_2 suggests that these nanosheets with smaller lateral dimensions are thin to around 2 nm corresponding to 3 or 4 monolayers of MoS_2. Meanwhile, the thickness obtained from Figure 2f is representative considering the very similar contrast between the selected dots and other dots.

Compared with the black green MoS_2 supernatant collected by centrifugation at 3000 rpm (Inset in Figure 3a), the as-prepared supernatant at 11000 rpm containing a high concentration of smaller MoS_2 nanosheets appears to be amber in color, as shown in the inset image in Figure 3b. These supernatants were very stable, and precipitation was scarcely observed over period of several months. Further investigation on the optical properties of the prepared MoS_2 nanosheets was performed by measuring their UV−vis absorption spectra. The UV−vis spectrum of MoS_2 supernatant at 11000 rpm exhibits four optical absorption peaks at 390, 440, 605, and 660 nm, which are in accordance with the characteristic peaks of exfoliated MoS_2 with smaller lateral dimensions.[49−52] The weak excitonic peaks at 605 and 660 nm are ascribed to the K point of the Brillouin zone in 2D MoS_2 with larger lateral dimensions.[33,50] The weak features of these peaks are due to the small concentration of the relatively larger 2D sheets in the supernatants (as evidenced in Figure 2d). Besides the two weak peaks, an obvious peak at 390 nm and a less prominent shoulder peak at 440 nm could be assigned to the direct transition from the deep valence band to the conduction band.[11,53] In addition, we also found a strongly blue shift in the optical absorption in comparison to those of MoS_2 nanosheets with relatively larger lateral dimensions (Figure 3a), arising from the quantum size effect of MoS_2 nanosheets with smaller lateral dimensions.

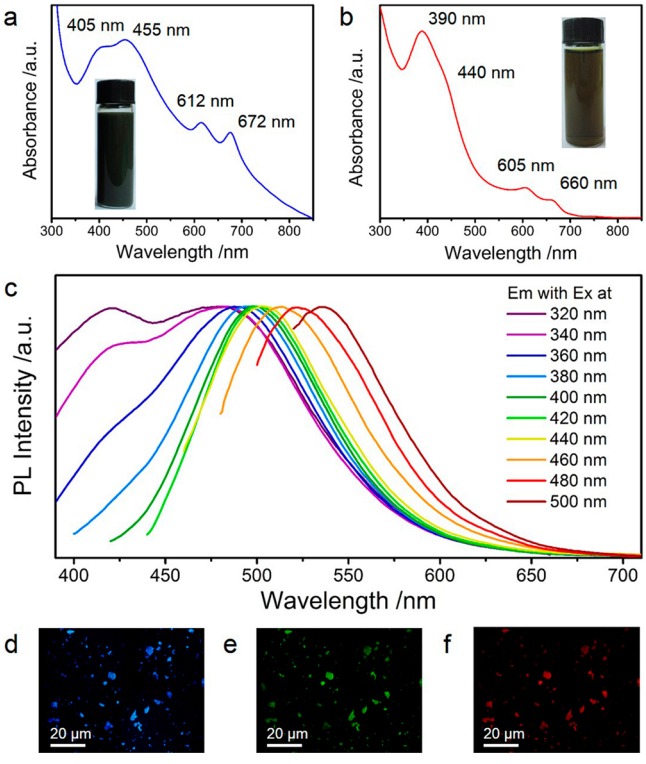

Figure 3. (a) Absorption spectra of MoS_2 supernatants collected by centrifugation at 3000 rpm. (b) Absorption spectra of MoS_2 supernatants collected by centrifugation at 11000 rpm. (c) PL spectra of as-prepared MoS_2 supernatants at 11000 rpm under excitation wavelengths of 320−500 nm. The fluorescent images of dried MoS_2 sheets at broadband excitation light sources of (d) UV (300−400 nm), (e) blue (400−500 nm), and (f) green (500−600 nm).

Since the PL properties of 2D MoS_2 sheets are a strong function of their lateral dimensions because of the quantum size effect,[51,52] for the MoS_2 nanosheets below 120 nm, their PL properties are supposed to differ from those with relatively larger lateral dimensions of micrometers.[33−35] The PL spectra using fluorescence spectroscopy at various excitation wavelengths ranging from 320 to 500 nm are measured to provide the PL properties of the 2D nanosheets with smaller lateral dimensions. Compared with the PL peaks of MoS_2 nanosheets with relatively larger lateral dimensions,[33−35] these PL peaks shown in Figure 3c occur the strongly blue shifts, which are in accordance with those of low-dimensional liquid exfoliated MoS_2 sheets with smaller lateral dimensions,[49−52] possibly because of the quantum size effect. It is also observed that the increase in the excitation wavelength from 320 to 500 nm leads to a red shift in the PL spectra of the nanosheets over emission wavelengths ranging from 480 to 540 nm. This observation suggests that the excitation dependent PL is associated with the polydispersity of the 2D MoS_2 nanosheets. For the excitation wavelength of 320 nm, besides a strong emission peak at 480 nm, a shoulder emission at 420 nm appears and generates a red shift with the excitation wavelengths from 320 to 380 nm. In addition, by the analysis of fluorescence microscope, similar phenomena were observed in our dried MoS_2 sheets consisting of small-size MoS_2 nanosheets that the as-fabricated MoS_2 exhibit the blue, green, and red emission under the excitation of the light sources of UV, blue, and green, respectively (Figure 3d−f).

The extraordinary PL properties of MoS_2 nanosheets with smaller lateral dimensions (below 120 nm) make it have great potential in optoelectronic and biological applications. However, for the biological applications including cell-targeted labeling, cell tracking and gene technology, it is important to ensure the good biocompatibility and nontoxicity of nanomaterials. Human U251 glioblastoma cells are used as the model to evaluate the cytotoxicity, cell viability and programmed cell death after incubation. Figure 4 shows that the U251 glioblastoma cells treated with MoS_2 nonosheets with smaller lateral dimensions (blow 120 nm) ranging from 25 to 500 μg/mL generally exhibited a comparable proliferation activity in contrast with the cells untreated with MoS_2, which indicates that low doses of MoS_2 nanosheets (25−500 μg/mL) were nontoxic to these cells and the proliferation capacity of the U251 glioblastoma cells is not affected by MoS_2 nanosheets at the testing concentrations with prolonged exposure times. In

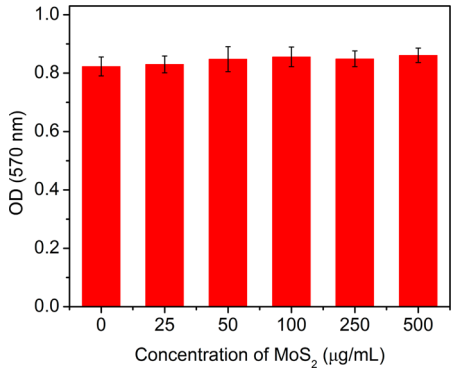

Figure 4. Cell viability assay with human U251 glioblastoma cells treated with different concentrations of MoS_2 nanosheets with smaller lateral dimensions below 120 nm. The bars represent cell counts and the error bars represent standard errors of the mean (SEM).

Figure 5, it is also observed that the U251 glioblastoma cells treated with MoS_2 nanosheets exhibited intact viability

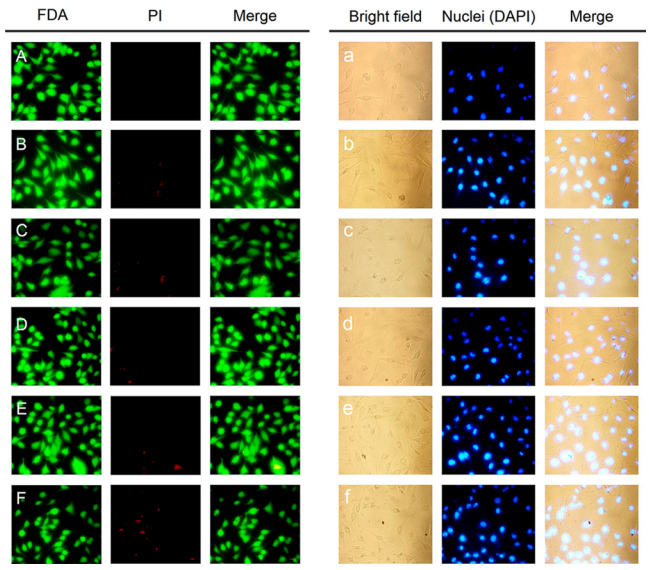

Figure 5. Assays of cell viability and apoptosis of the treated U251 glioblastoma cells with MoS_2 nanosheets with smaller lateral dimensions. The untreated U251 cells are used as controls (A, a) and the images (B–F, b–f) are the treated U251 glioblastoma cells with MoS_2 nanosheets of various concentrations (including 25, 50, 100, 250, 500 μg/mL).

compared with the U251 cells without MoS_2 treatment. Simultaneously, as shown in Figure 5, the nuclear fragmentation and chromatin condensation were not detected in the cells treated with at the testing concentrations of MoS_2 nonosheets, clearly indicating that the treatment of MoS_2 nanosheets does not induce programmed cell death in U251 glioblastoma cells.

To explore the potential in cell-targeted labeling applications, MoS_2 nanosheets with smaller lateral dimensions below 120 nm used as fluorescent labels to perform cellular labeling. The cellular imaging of these MoS_2 nanosheets with smaller lateral dimensions was performed on lung cancer cells. Before labeling, cells were incubated with MoS_2 nanosheets with smaller lateral dimensions at 37 °C for 24 h. More detailed preparation methods can be found in the Experimental Section. In the lung cancer cells stained with MoS_2, the nanosheets with smaller dimensions were taken up by the cells and agglomerated in the cells. Figure 6a–c shows the fluorescent images of lung cancer cells stained with MoS_2 nanosheets with smaller dimensions at

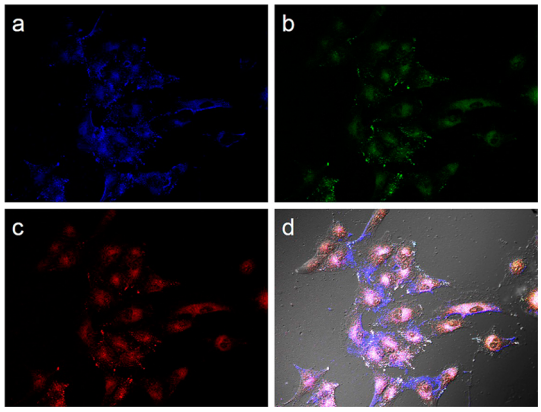

Figure 6. Fluorescent images of lung cancer cells stained with MoS_2 nanosheets with smaller lateral dimensions at broadband excitation light sources of (b) UV (300–400 nm), (c) blue (400–500 nm), and (d) green (500–600 nm). (a) The overlay image of panels a, b, and c and bright-field image.

broadband excitation light sources of UV (300–400 nm), blue (400–500 nm), and green (500–600 nm), exhibiting the blue, green, and red emission, respectively. In Figure 6d, the overlay image clearly shows that the strongly fluorescent MoS_2 nanosheets were taken up by the cytoplasm but did not penetrate the cell nuclei, and the boundary between cells, nuclei, and cytoplasm is clear. It suggests that MoS_2 nanosheets with smaller lateral dimensions can be used in high contrast cell-targeted labeling and will be well-suited for other biomedical applications.

4. CONCLUSIONS

In summary, polydisperse MoS_2 nanosheets have been synthesized from natural molybdenite in the emulsions microenvironment built by the water/surfactant/CO_2 system. By adjusting the centrifugation rate, the MoS_2 nanosheets with various dimensional sizes can be successfully selected. The nanosheets with small size are thin to around 2 nm corresponding to 3 or 4 monolayers can be successfully achieved. Because of their quantum size effect, the obtained MoS_2 nanosheets exhibit extraordinary photoluminescence properties. Further evaluation indicates their good biocompatibility and nontoxicity to cells. By the cell staining assay and the fluorescence microscope, we successfully demonstrate the employment of PL properties of MoS_2 nanosheets with smaller lateral dimensions in cell-targeted labeling applications.

■ ASSOCIATED CONTENT

Ⓢ Supporting Information

TEM images of MoS_2 nanosheets with smaller lateral dimensions and AFM image of MoS_2 and Raman spectra of the few-layer and bulk MoS_2. All these information are available free of charge via the Internet at http://pubs.acs.org/.

■ AUTHOR INFORMATION

Corresponding Author

*Fax: +86 371 67767827. Tel.: +86 371 67767827. E-mail: qunxu@zzu.edu.cn.

Notes

The authors declare no competing financial interest.

■ ACKNOWLEDGMENTS

We are grateful for the National Natural Science Foundation of China (Nos. 51173170, 50955010, and 20974102), the financial support from the Innovation Talents Award of Henan Province (114200510019) and the Program for New Century Excellent Talents in University (NCET-08-0667).

■ REFERENCES

(1) Huang, X.; Tan, C. L.; Yin, Z. Y.; Zhang, H. 25th Anniversary Article: Hybrid Nanostructures Based on Two-Dimensional Nanomaterials. *Adv. Mater.* **2014**, *26*, 2185−2204.
(2) Geim, A. K. Graphene: Status and Prospects. *Science* **2009**, *324*, 1530−1534.
(3) Novoselov, K. S.; Jiang, D.; Schedin, F.; Booth, T. J.; Khotkevich, V. V.; Morozov, S. V.; Geim, A. K. Two-Dimensional Atomic Crystals. *Proc. Natl. Acad. Sci. U.S.A.* **2005**, *102*, 10451−10543.
(4) Nicolosi, V.; Chhowalla, M.; Kanatzidis, M. G.; Strano, M. S.; Coleman, J. N. Liquid Exfoliation of Layered Materials. *Science* **2013**, *340*, 1420−1438.
(5) Novoselov, K. S.; Fal'ko, V. I.; Colombo, L.; Gellert, P. R.; Schwab, M. G.; Kim, K. A Roadmap for Graphene. *Nature* **2012**, *490*, 192−200.
(6) Chhowalla, M.; Shin, H. S.; Eda, G.; Li, L.-J.; Loh, K. P.; Zhang, H. The Chemistry of Two-Dimensional Layered Transition Metal Dichalcogenide Nanosheets. *Nat. Chem.* **2013**, *5*, 263−275.
(7) Huang, X.; Zeng, Z. Y.; Fan, Z. X.; Liu, J. Q.; Zhang, H. Graphene-Based Electrodes. *Adv. Mater.* **2012**, *24*, 5979−6004.
(8) Ganatra, R.; Zhang, Q. Few-Layer MoS_2: A Promising Layered Semiconductor. *ACS Nano* **2014**, *8*, 4074−4099.
(9) Radisavljevic, B.; Radenovic, A.; Brivio, J.; Giacometti, V.; Kis, A. Single-Layer MoS_2 Transistors. *Nat. Nanotechnol.* **2011**, *6*, 147−150.
(10) Lee, K.; Kim, H.-Y.; Lotya, M.; Coleman, J. N.; Kim, G.-T.; Duesberg, G. S. Electrical Characteristics of Molybdenum Disulfide Flakes Produced by Liquid Exfoliation. *Adv. Mater.* **2011**, *23*, 4178−4182.
(11) Wilson, J. A.; Yoffe, A. D. The Transition Metal Dichalcogenides Discussion and Interpretation of Optical, Electrical and Structural Properties. *Adv. Phys.* **1969**, *18*, 193−335.
(12) Huang, X.; Zeng, Z. Y.; Zhang, H. Metal Dichalcogenide Nanosheets: Preparation, Properties and Applications. *Chem. Soc. Rev.* **2013**, *42*, 1934−1946.
(13) Cunningham, G.; Lotya, M.; Cucinotta, C. S.; Sanvito, S.; Bergin, S. D.; Menzel, R.; Shaffer, M. S. P.; Coleman, J. N. Solvent Exfoliation of Transition Metal Dichalcogenides: Dispersibility of Exfoliated Nanosheets Varies Only Weakly Between Compounds. *ACS Nano* **2012**, *6*, 3468−3480.
(14) Eda, G.; Fujita, T.; Yamaguchi, H.; Voiry, D.; Chen, M. W.; Chhowalla, M. Coherent Atomic and Electronic Heterostructures of Single-Layer MoS_2. *ACS Nano* **2012**, *6*, 7311−7317.
(15) Mattheiss, L. F. Band Structures of Transition-Metal-Dichalcogenide Layer Compounds. *Phys. Rev. B* **1973**, *8*, 3719−3740.
(16) Li, H.; Wu, J.; Yin, Z. Y.; Zhang, H. Preparation and Applications of Mechanically Exfoliated Single-Layer and Multilayer MoS_2 and WSe_2 Nanosheets. *Acc. Chem. Res.* **2014**, *47*, 1067−1075.
(17) Smith, R. J.; King, P. J.; Lotya, M.; Wirtz, C.; Khan, U.; De, S.; O'Neill, A.; Duesberg, G. S.; Grunlan, J. C.; Moriarty, G.; Chen, J.; Wang, J. Z.; Minett, A. I.; Nicolosi, V.; Coleman, J. N. Large-Scale Exfoliation of Inorganic Layered Compounds in Aqueous Surfactant Solutions. *Adv. Mater.* **2011**, *23*, 3944−3948.
(18) Coleman, J. N.; Lotya, M.; O'Neill, A.; Bergin, S. D.; King, P. J.; Khan, U.; Young, K.; Gaucher, A.; De, S.; Smith, R. J.; Shvets, I. V.; Arora, S. K.; Stanton, G.; Kim, H.-Y.; Lee, K.; Kim, G. T.; Duesberg, G. S.; Hallam, T.; Boland, J. J.; Wang, J. J.; Donegan, J. F.; Grunlan, J. C.; Moriarty, G.; Shmeliov, A.; Nicholls, R. J.; Perkins, J. M.; Grieveson, E. M.; Theuwissen, K.; McComb, D. W.; Nellist, P. D.; Nicolosi, V. Two-Dimensional Nanosheets Produced by Liquid Exfoliation of Layered Materials. *Science* **2011**, *331*, 568−571.
(19) Zhou, K.-G.; Mao, N.-N.; Wang, H.-X.; Peng, Y.; Zhang, H.-L. A Mixed-Solvent Strategy for Efficient Exfoliation of Inorganic Graphene Analogues. *Angew. Chem., Int. Ed.* **2011**, *50*, 10839−10842.
(20) Liu, J. Q.; Zeng, Z. Y.; Cao, X. H.; Lu, G.; Wang, L.-H.; Fan, Q.-L.; Huang, W.; Zhang, H. Preparation of MoS_2-Polyvinylpyrrolidone Nanocomposites for Flexible Nonvolatile Rewritable Memory Devices with Reduced Graphene Oxide Electrodes. *Small* **2012**, *8*, 3517−3522.
(21) Yao, Y. G.; Tolentino, L.; Yang, Z. Z.; Song, X. J.; Zhang, W.; Chen, Y. S.; Wong, C.-P. High-Concentration Aqueous Dispersions of MoS_2. *Adv. Funct. Mater.* **2013**, *23*, 3577−3583.
(22) Frey, G. L.; Reynolds, K. J.; Friend, R. H.; Cohen, H.; Feldman, Y. Solution-Processed Anodes from Layer-Structure Materials for High-Efficiency Polymer Light-Emitting Diodes. *J. Am. Chem. Soc.* **2003**, *125*, 5998−6007.
(23) Joensen, P.; Frindt, R. F.; Morrison, S. R. Single-Layer MoS_2. *Mater. Res. Bull.* **1986**, *21*, 457−461.
(24) Zeng, Z. Y.; Sun, T.; Zhu, J. X.; Huang, X.; Yin, Z. Y.; Lu, G.; Fan, Z. X.; Yan, Q. Y.; Hng, H. H.; Zhang, H. An Effective Method for the Fabrication of Few-Layer-Thick Inorganic Nanosheets. *Angew. Chem., Int. Ed.* **2012**, *51*, 9052−9056.
(25) Wang, Q. H.; Kalantar−Zadeh, K.; Kis, A.; Coleman, J. N.; Strano, M. S. Electronics and Optoelectronics of Two-Dimensional Transition Metal Dichalcogenides. *Nat. Nanotechnol.* **2012**, *7*, 699−712.
(26) Zhang, Y.; Ye, J.; Matsuhashi, Y.; Iwasa, Y. Ambipolar MoS_2 Thin Flake Transistors. *Nano Lett.* **2012**, *12*, 1136−1140.
(27) Radisavljevic, B.; Whitwick, M. B.; Kis, A. Integrated Circuits and Logic Operations Based on Single-Layer MoS_2. *ACS Nano* **2011**, *5*, 9934−9938.
(28) Zeng, Z. Y.; Yin, Z. Y.; Huang, X.; Li, H.; He, Q. Y.; Lu, G.; Boey, F.; Zhang, H. Single-Layer Semiconducting Nanosheets: High-Yield Preparation and Device Fabrication. *Angew. Chem., Int. Ed.* **2011**, *50*, 11093−11097.
(29) Li, H.; Yin, Z. Y.; He, Q. Y.; Li, H.; Huang, X.; Lu, G.; Fam, D. W. H.; Tok, A. I. Y.; Zhang, Q.; Zhang, H. Fabrication of Single- and Multilayer MoS_2 Film-Based Field-Effect Transistors for Sensing NO at Room Temperature. *Small* **2012**, *8*, 63−67.
(30) Stephenson, T.; Li, Z.; Olsenab, B.; Mitlin, D. Lithium Ion Battery Applications of Molybdenum Disulfide (MoS_2) Nanocomposites. *Energy Environ. Sci.* **2014**, *7*, 209−231.
(31) Laursen, L. B.; Kegnæs, S.; Dahla, S.; Chorkendorff, I. Molybdenum Sulfides Efficient and Viable Materials for Electro- and Photoelectrocatalytic Hydrogen Evolution. *Energy Environ. Sci.* **2012**, *5*, 5577−5591.
(32) Karunadasa, H. I.; Montalvo, E.; Sun, Y. J.; Majda, M.; Long, J. R.; Chang, C. J. A Molecular MoS_2 Edge Site Mimic for Catalytic Hydrogen Generation. *Science* **2012**, *335*, 698−702.
(33) Mak, K. F.; Lee, C.; Hone, J.; Shan, J.; Heinz, T. F. Atomically Thin MoS_2: A New Direct-Gap Semiconductor. *Phys. Rev. Lett.* **2010**, *105*, 136805−136808.
(34) Eda, G.; Yamaguchi, H.; Voiry, D.; Fujita, T.; Chen, M. W.; Chhowalla, M. Photoluminescence from Chemically Exfoliated MoS_2. *Nano Lett.* **2011**, *11*, 5111−5116.
(35) Splendiani, A.; Sun, L.; Zhang, Y. B.; Li, T. S.; Kim, J.; Chim, C.-Y.; Galli, G.; Wang, F. Emerging Photoluminescence in Monolayer MoS_2. *Nano Lett.* **2010**, *10*, 1271−1275.
(36) Yin, Z. Y.; Li, H.; Li, H.; Jiang, L.; Shi, Y. M.; Sun, Y. H.; Lu, G.; Zhang, Q.; Chen, X. D.; Zhang, H. Single-Layer MoS_2 Phototransistors. *ACS Nano* **2012**, *6*, 74−80.
(37) Li, Y.; Wang, H.; Xie, L.; Liang, Y.; Hong, G.; Dai, H. MoS_2 Nanoparticles Grown on Graphene: An Advanced Catalyst for the Hydrogen Evolution Reaction. *J. Am. Chem. Soc.* **2011**, *133*, 7296−7299.
(38) Voiry, D.; Salehi, M.; Silva, R.; Fujita, T.; Chen, M.; Asefa, T.; Shenoy, V. B.; Eda, G.; Chhowalla, M. Conducting MoS_2 Nanosheets as Catalysts for Hydrogen Evolution Reaction. *Nano Lett.* **2013**, *13*, 6222−6227.

(39) Wang, H.; Lu, Z.; Xu, S.; Kong, D.; Cha, J. J.; Zheng, G.; Hsu, P.-C.; Yan, K.; Bradshaw, D.; Prinz, F. B.; Cui, Y. Electrochemical Tuning of Vertically Aligned MoS_2 Nanofilms and Its Application in Improving Hydrogen Evolution Reaction. *Proc. Natl. Acad. Sci. U.S.A.* **2013**, *110*, 19701−19706.
(40) Lin, L. X.; Xu, Y. X.; Zhang, S. W.; Ross, I. M.; Ong, A. C. M.; Allwood, D. A. Fabrication of Luminescent Monolayered Tungsten Dichalcogenides Quantum Dots with Giant Spin-Valley Coupling. *ACS Nano* **2013**, *7*, 8214−8223.
(41) Sarkar, D.; Liu, W.; Xie, X. J.; Anselmo, A. C.; Mitragotri, S.; Banerjee, K. MoS_2 Field-Effect Transistor for Next-Generation Label-Free Biosensors. *ACS Nano* **2014**, *8*, 3992−4003.
(42) Liu, T.; Wang, C.; Gu, X.; Gong, H.; Cheng, L.; Shi, X. Z.; Feng, L. Z.; Sun, B. Q.; Liu, Z. Drug Delivery with PEGylated MoS_2 Nanosheets for Combined Photothermal and Chemotherapy of Cancer. *Adv. Mater.* **2014**, *8*, 3992−4012.
(43) Zhu, C. F.; Zeng, Z. Y.; Li, H.; Li, F.; Fan, C. H.; Zhang, H. Single-Layer MoS_2-Based Nanoprobes for Homogeneous Detection of Biomolecules. *J. Am. Chem. Soc.* **2013**, *135*, 5998−6001.
(44) Ge, J.; Ou, E.-C.; Yu, R.-Q.; Chu, X. A Novel Aptameric Nanobiosensor Based on the Self-Assembled DNA-MoS_2 Nanosheet Architecture for Biomolecule Detection. *J. Mater. Chem. B* **2014**, *2*, 625−628.
(45) Chou, S. S.; Kaehr, B.; Kim, J.; Foley, B. M.; De, M.; Hopkins, P. E.; Huang, J.; Brinker, C. J.; Dravid, V. P. Chemically Exfoliated MoS_2 as Near-Infrared Photothermal Agents. *Angew. Chem., Int. Ed.* **2013**, *125*, 4254.
(46) Lee, C. T., Jr.; Psathas, P. A.; Johnston, K. P. Water-in-Carbon Dioxide Emulsions: Formation and Stability. *Langmuir* **1999**, *15*, 6781−6791.
(47) Eckert, Ca.; Knutson, B. L.; Debenedetti, P. G. Supercritical Fluids as Solvents for Chemical and Materials Processing. *Nature* **1996**, *383*, 313−318.
(48) Johnston, K. P.; Harrison, K. L.; Clarke, M. J.; Howdle, S. M.; Heitz, M. P.; Bright, F. V.; Carlier, C.; Randolph, T. W. Water-in-Carbon Dioxide Microemulsions: An Environment for Hydrophiles Including Proteins. *Science* **1996**, *271*, 624−626.
(49) Gopalakrishnan, D.; Damien, D.; Shaijumon, M. M. MoS_2 Quantum Dot-Interspersed Exfoliated MoS_2 Nanosheets. *ACS Nano* **2014**, *8*, 5297−5303.
(50) Wang, Y.; Ou, J. Z.; Balendhran, S.; Chrimes, A. F.; Mortazavi, M.; Yao, D. D.; Field, M. R.; Latham, K.; Bansal, V.; Friend, J. R.; Zhuiykov, S.; Medhekar, N. V.; Strano, M. S.; Kalantar-zadeh, K. Electrochemical Control of Photoluminescence in Two-Dimensional MoS_2 Nanoflakes. *ACS Nano* **2013**, *7*, 10083−10093.
(51) Ou, J. Z.; Chrimes, A. F.; Wang, Y. C.; Tang, S.-Y.; Strano, M. S.; Kalantar-zadeh, K. Ion-Driven Photoluminescence Modulation of Quasi-Two Dimensional MoS_2 Nanoflakes for Applications in Biological Systems. *Nano Lett.* **2014**, *14*, 857−863.
(52) Stengl, V.; Henych, J. Strongly Luminescent Monolayered MoS_2 Prepared by Effective Ultrasound Exfoliation. *Nanoscale* **2013**, *5*, 3387−3394.
(53) Wilcoxon, J. P.; Samara, G. A. Strong Quantum-Size Effects in a Layered Semiconductor: MoS_2 Nanoclusters. *Phys. Rev. B* **1995**, *51*, 7299−7203.
(54) Napierska, D.; Thomassen, L. C.; Rabolli, V.; Lison, D.; Gonzalez, L.; Kirsch-Volders, M.; Martens, J. A.; Hoet, P. H. Size-Dependent Cytotoxicity of Monodisperse Silica Nanoparticles in Human Endothelial Cells. *Small* **2009**, *5*, 846−853.
(55) Wang, X.; Wei, F.; Liu, A.; Wang, L.; Wang, J. C.; Ren, L.; Liu, W.; Tu, Q.; Li, L.; Wang, J. Cancer Stem Cell Labeling Using Poly(L-lysine)-Modified Iron Oxide Nanoparticles. *Biomaterials* **2012**, *33*, 3719−3732.